Numerical Simulation of Turbulent Air Natural Convection in A U-Shaped Channel

Touta Hadji[1*], Riad Hadjab[1] , Aissa Abidi-Saad[1]

[1]Faculté des Hydrocarbures et Energies renouvelables et Sciences de la terre et de l'univers, Université Kasdi Merbah, 30000 Ouargla, Algérie

*e-mail: hadji.touta2015@gmail.com

Received: 02/06/2022; Accepted: 05/10/2022; Published: 31/10/2022

Abstract

In this study a turbulent air-natural convection in a U-shaped channel under asymmetric heating conditions is investigated numerically. The heated channel comprises two insulated walls and two heated walls. One wall is directly heated at a constant temperature ranging from 50 to 500 °C, while the other wall is indirectly heated through thermal radiation emitted from the directly heated wall. The governing equations were solved using the Computational Fluid Dynamics (CFD) software, FLUENT. The temperature-dependent physical properties of the air were integrated using the "User Defined Functions". The numerical results were validated against existing experimental data, showing a good agreement. Also, the impact of varying Directly Heated Wall (DHW) temperatures on parameters such as air temperature, air velocity, heat removal, and the Nusselt number has been examined. The findings offer valuable insights that can be used to optimize the design of natural convection systems across various applications.

Keywords: natural convection; turbulent flow; U-shaped channel; Fluent CFD

Tob Regul Sci.™ 2022;8(2): 664 - 678

DOI: doi.org/10.18001/TRS.8.2.44

1. Introduction

Heat flow studies nowadays, air natural convection systems are gaining more attention for their energy efficiency and sustainability. In applications like chimneys in buildings, heat sinks of electronic components and radiators using large parallel fins, heat transfer behavior between components can be simplified as natural convection between parallel plates. Plate orientation and thermal boundary conditions affect significantly heat transfer and flow patterns in channels. Extensive research, both experimental and numerical, has been conducted on heat transfer between parallel plates over several decades. Elenbaas [1] and Bodoia and Osterle [2] were the pioneers in studying symmetrically heated isothermal plates, while Ostrach [3], Aung [4], Miyatake et al.[5], Nelson and Wood [6] and Yilmaz, and Gilchrist [7] explored vertical parallel plates with asymmetric heating conditions. Authors have reported numerous correlations between the Nusselt number, Rayleigh number and aspect ratio to predict heat transfer rates. These correlations are highly dependent on the surface conditions of the plates, including whether they are symmetric or asymmetric, and subject to isothermal or isoflux conditions. Bar-Cohen and Rohsenow [8] obtained a correlation which can be applied to a wide range of aspect ratios by combining the

correlations for the isolated plate conditions and the fully developed limit. From this correlation, it is possible to obtain optimal plate spacing, which maximizes the heat transfer for an array of isothermal vertical plates. Cheng and Müller [9] investigated both numerically and experimentally turbulent natural convection in an asymmetric heated channel coupled with thermal radiation. They showed that at intermediate and high wall emissivity thermal radiation contributes significantly to the total heat transfer by natural air convection, even at low temperatures of the heated wall. Finally, they developed a correlation for the Nusselt number in terms of convective and radiative heat transfers. Cadafalch et al. [10] performed experimental and numerical simulations to study heat transfer in large, inclined channels with asymmetric heating and surface radiation. The authors studied several factors such as: variations in channel length, inter-plate spacing, inclination angle, emissivity of the plates, and temperature difference between the isothermal wall and the ambient. They obtained correlations for the Nusselt number in terms of the surface emissivity and modified Rayleigh number including the channel aspect ratio and the inclination angle. Desrayaud and Fichera [11] conducted a numerical investigation of laminar natural convection flows in a vertical isothermal channel with two rectangular ribs. They analyzed the effect of the ribs' location, conductivity, and size on the heat transfer and flow patterns. Based on numerical simulations, Khanal and Lei [12] proposed a solar chimney design with a horizontal inlet. Their design features an inclined passive wall aimed to reduce the flow reversal and improve ventilation. They determined the maximum mass flow rate by optimizing the inclination angle for a given Rayleigh number. Gan [13] used a CFD model to predict airflow patterns and heat transfer rates in channels under asymmetric heating conditions, considering two types based on inlet position, whether vertical or horizontal. Correlations have been obtained in terms of Nusselt, Reynolds, Rayleigh numbers and aspect ratio. In their study, Kim et al. [14] experimentally investigated the turbulent air natural convection between vertical parallel plates with asymmetric heating, using a rectangular air channel with insulated and heated walls. They visualized the absence of reverse flow at the outlet and showed a deviation between mean and measured air temperatures at the channel center. In addition, from their experimental results, they suggested two distinct recirculation flow patterns and proposed two correlations for natural convection heat transfer.

In the current paper, we present a numerical simulation of turbulent air natural convection in U-shaped channel subjected to asymmetric heating conditions, as depicted in Figure 1.a. This U-shaped channel replicates the geometry employed by Kim et al. [14], to validate our numerical results with their experimental findings. It's worth noting the scarcity of numerical and experimental studies on natural convection in channels with wall temperatures exceeding 200°C. Hence, our numerical study covers a broad range of wall temperatures (50–500°C) as performed experimentally by Kim et al. [14]. Temperature-dependent air properties are adopted to address the momentum, energy, and turbulence equations. The simulation results are compared with the experimental measurements reported by Kim et al. [14], encompassing temperature and velocity distributions and heat removal rates through both natural convection and radiation.

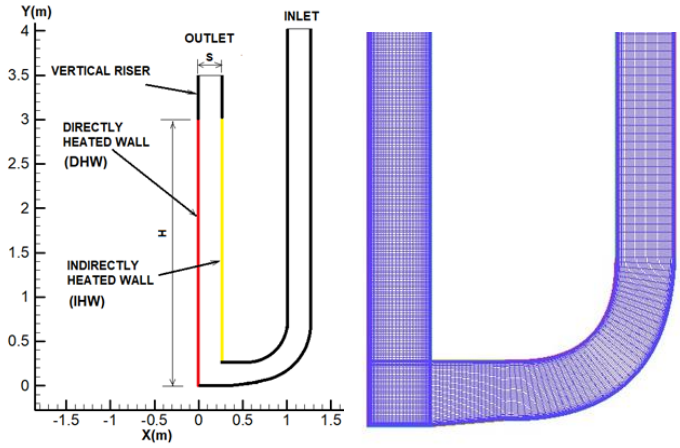

Figure 1. Description of (a) geometry and boundary condition, (b) used mesh

2. Model formulation

2.1. Geometry description and assumptions:

- The configuration of U-shaped channel consisted of two insulated walls with a height of 4.0 m on the right side, two heated walls with a height of 3.0 mand an aspect ratio (S/H) of 0.0883 on the left side, an insulated vertical riser with a height of 0.5 m and an insulated horizontal connector of 1.0 m, as shown in fig. 1.a.

- The left wall DHW, highlighted in red, was uniformly heated at constant temperature ranging between 500°C and 50°C. The right wall IHW, highlighted in yellow, was indirectly heated by radiative heat received from (DHW).

- Both DHW and IHW walls are composed of stainless steel with identical emissivity ϵ.

- The flow through the channels is entirely induced by buoyancy, where cold air is drawn into the channel at the inlet under the ambient conditions, and the heated air is released into the ambient at the outlet.

- There is no thermal mixing of the inlet and outlet of the channel.

- The airflow and heat transfer processes are turbulent and transient.

- The ambient air temperature entering the inlet is maintained at T0=25 °C.

- The density of air changes with temperature using the ideal gas law as follows:

$$\rho(T) = \frac{P_o}{r_{air}.T} \quad (1)$$

- Other properties such as dynamic viscosity, thermal conductivity, and specific heat capacity also depend on temperature and are determined using the following equations, respectively [15]:

$$\mu(T) = 3.2575 \times 10^{-5} - 7.56163 \times 10^{-7}.T + 7.47253 \times 10^{-9}.T^2 - 2.86507 \times 10^{-11}.T^3 + 3.89067 \times 10^{-14}.T^4 \quad (2)$$

$$\lambda(T) = -3.06000 \times 10^{-4} + 9.89089 \times 10^{-5}.T - 3.46571 \times 10^{-6}.T^2 \quad (3)$$

$$Cp(T) = 1178.8 - 2.8765.T + 1.8105 \times 10^{-2}.T^2 - 5.1000 \times 10^{-5}.T^3 + 5.4000 \times 10^{-8}.T^4 \quad (4)$$

- The emissivity of the polished stainless steel is dependent on temperature using the following relationship derived from a reference curve[16]:

$$\epsilon(T) = 0.17812 - 6.12677 \times 10^{-5}.T + 5.51186 \times 10^{-8}.T^2 + 1.08033 \times 10^{-10}.T^3, \quad 300 < T < 773\ K \quad (5)$$

2.2. Governing equations:

In order to simulate the flow and heat transfer, two-dimensional realizable k-ε turbulence models are applied. The governing equations can be expressed as follows:

- Continuity equation: $\frac{\partial(\rho u)}{\partial x} + \frac{\partial(\rho v)}{\partial y} = 0$ (6)

- X-Momentum equation:

$$\rho\frac{\partial u}{\partial t} + \rho u\frac{\partial u}{\partial x} + \rho v\frac{\partial u}{\partial y} = -\frac{\partial p}{\partial x} + \frac{\partial}{\partial x}\left((\mu_t + \mu)\frac{\partial u}{\partial x}\right) + \frac{\partial}{\partial y}\left((\mu_t + \mu)\frac{\partial u}{\partial y}\right) \quad (7)$$

- Y-Momentum equation:

$$\rho\frac{\partial v}{\partial t} + \rho u\frac{\partial v}{\partial x} + \rho v\frac{\partial v}{\partial y} = -\frac{\partial p}{\partial y} + \frac{\partial}{\partial x}\left((\mu_t + \mu)\frac{\partial v}{\partial x}\right) + \frac{\partial}{\partial y}\left((\mu_t + \mu)\frac{\partial v}{\partial y}\right) + (\rho - \rho_0)g \quad (8)$$

- Turbulent kinetic energy k equation:

$$\rho\frac{\partial k}{\partial t} + \rho u\frac{\partial k}{\partial x} + \rho v\frac{\partial k}{\partial y} = \frac{\partial}{\partial x}\left(\left(\mu + \frac{\mu_t}{\sigma_k}\right)\frac{\partial k}{\partial x}\right) + \frac{\partial}{\partial y}\left(\left(\mu + \frac{\mu_t}{\sigma_k}\right)\frac{\partial k}{\partial y}\right) + G_k + G_b - \rho\varepsilon \quad (9)$$

- Rate of energy dissipation ε equation:

$$\rho\frac{\partial \varepsilon}{\partial t} + \rho u\frac{\partial \varepsilon}{\partial x} + \rho v\frac{\partial \varepsilon}{\partial y} = \frac{\partial}{\partial x}\left(\left(\mu + \frac{\mu_t}{\sigma_\varepsilon}\right)\frac{\partial \varepsilon}{\partial x}\right) + \frac{\partial}{\partial y}\left(\left(\mu + \frac{\mu_t}{\sigma_\varepsilon}\right)\frac{\partial \varepsilon}{\partial y}\right) + \rho C_1 S\varepsilon - \rho C_2\frac{\varepsilon^2}{k + \sqrt{\nu\varepsilon}} + C_{1\varepsilon}\frac{\varepsilon}{k}C_{3\varepsilon}G_b \quad (10)$$

Where:G_k represents the generation of turbulence kinetic energy due to the mean velocity gradients and is given by: $G_k = -\rho\overline{u_i'u_j'}\frac{\partial u_i}{\partial x_j} = \mu_t S^2$ where:$\mu_t = \rho C_\mu \frac{k^2}{\varepsilon}$ (11)

Gb is generation of turbulent kinetic due to buoyancy given by:

$$G_b = \beta g \frac{\mu_t}{\sigma_t}\frac{\partial T}{\partial y} \quad (12)$$

The coefficients related to the model are given as follows:

$$\eta = S\frac{k}{\varepsilon}, \qquad S = \sqrt{2S_{ij}S_{ij}}, \qquad S_{ij} = \frac{1}{2}\left(\frac{\partial u_j}{\partial x_i} + \frac{\partial u_i}{\partial x_j}\right) \quad (13)$$

$$C_1 = \max\left[0.43, \frac{\eta}{\eta+5}\right], \quad C_2 = 1.9, \quad \sigma_k = 1.0, \sigma_\varepsilon = 1.2, \quad C_{1\varepsilon} = 1.44$$

- Energy equation:

$$c_p\rho\frac{\partial T}{\partial t} + c_p\rho u\frac{\partial T}{\partial x} + c_p\rho v\frac{\partial T}{\partial y} = \frac{\partial}{\partial x}\left(\left(\lambda + \frac{c_p\mu_t}{\sigma_t}\right)\frac{\partial T}{\partial x}\right) + \frac{\partial}{\partial y}\left(\left(\lambda + \frac{c_p\mu_t}{\sigma_t}\right)\frac{\partial T}{\partial y}\right) \quad (14)$$

2.3. Boundary conditions:

- At initial condition, the air is at rest: u = v = 0, T = T_0
- A no-slip boundary condition is imposed on the velocity components at the walls: u=v=0.
- At the channel inlet, the ambient air accelerates from rest to the induced velocity v_{in} and is specified as a gauge pressure outlet boundary condition :$p_{g,in} = -\frac{1}{2}\rho_0 v_{in}^2$, $T = T_0$ (15 – 25 °C)
- At the channel outlet, the heated air is specified as a gauge pressure outlet boundary condition : $p_{g,out} = 0$, $\frac{\partial T}{\partial y} = 0$
- Walls are set as adiabatic except for the wall DHW where the temperature remains uniform: $T=T_W$
- The temperature at the adiabatic wall IHW results from a surface energy balance considering that the net radiative heat flux arriving at the wall equals the heat flux transferred from the wall to the adjacent air: $\frac{\epsilon}{2-\epsilon}\sigma(T_w^4 - T^4) = -\lambda\frac{\partial T}{\partial x}$

The total heat removal rate from the channel is determined from the following equation:

$$\dot{Q}removal = \dot{m}.C_{p,avg}(Tout - Tin) \quad (15)$$

On the other hand, the total heat removal rate is the sum of the convective heat rate transported to the air, $\dot{Q}_{conv}$ and the net radiative heat rate transferred from the DHW to the IHW, $\dot{Q}_{Rad}$ which is determined with the discrete ordinates (DO) radiation model. Therefore, the convective heat rate is computed from the following equation:

$$\dot{Q}_{conv} = \dot{Q}_{removal} - \dot{Q}_{Rad} \quad (16)$$

The Rayleigh and Nusselt numbers are defined as follows:

$$Ra = \left[\frac{g\beta(T_w - T_0)S^3}{\nu^2}\right] Pr, \qquad Nu_{conv} = \frac{h.H}{\lambda} \qquad \text{Where: } h = \frac{Q_{conv}(T_w - T_0)}{A} \quad (17)$$

The computations of the governing equations are carried out using Fluent CFD code based on the finite-volume method. The algorithm employed is coupled scheme for pressure-velocity coupling and second order up-wind for spatial discretization. The physical properties of the air and the emissivity of the heated walls in eqs.(1)– (5) are incorporated as User Defined Functions. For modeling radiative heat transfer, discrete ordinates (DO) radiation model is chosen. It is used to model the transport of thermal radiation within participating media such as gases, liquids, and solids and provides a versatile and computationally efficient approach in a wide range of engineering applications [17]. In the present study, hexahedral mesh was chosen for the discretization using ICEM CFD, with a refined mesh implemented in the vicinity of the walls, as shown in figure 1.b.

3. Results and discussion

For the validation of our numerical model, the obtained numerical results of the configuration are compared with the experimental measurements and results performed by Kim et al. [14].The horizontal temperature profiles are computed at elevations of 0.9, 1.5, 2.1, and 2.7 m and juxtaposed with the corresponding measured temperature profiles for the DHW of 500°C case, as depicted in Fig. 2. The comparison between the numerical and the experimental results is largely satisfactory. This assessment is based on the area-weighted average temperature for each profile, as presented in Table 1, where minor discrepancies do not exceed 10%. An exception is noted near the DHW wall, where the measured temperatures don't coincide well with the numerical solutions. However, this discrepancy near the DHW wall does not compromise the overall agreement.

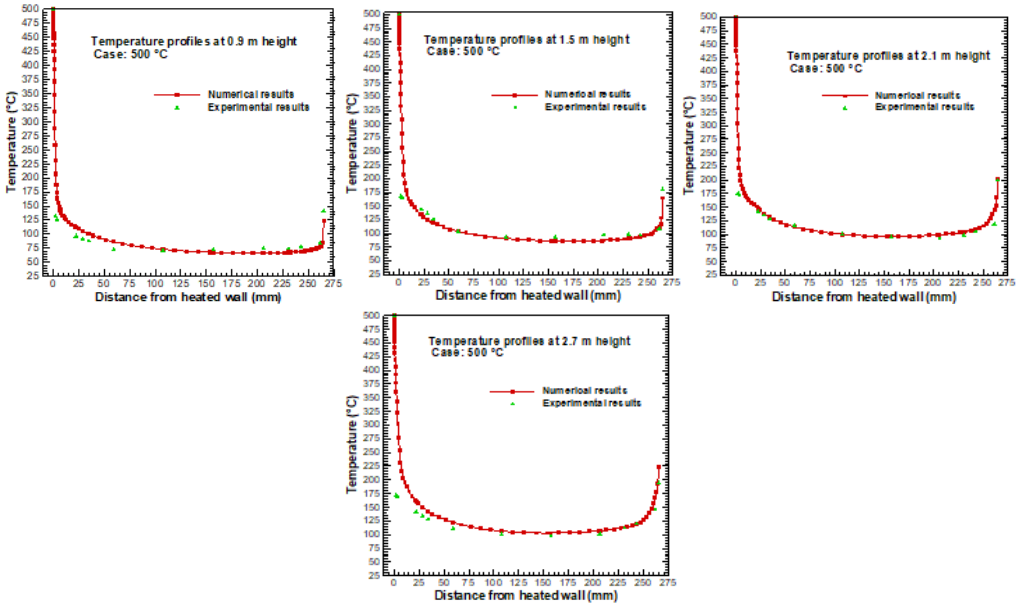

Figure 2: Numerical and measured temperature profiles for: 500°C case

Table.1: Average temperature for different heights on the channel: case 500°C

Height (m)	Tavg, Num(°C)	Tavg, Exp (°C)	Error %
0.9	81.13	78.11	3.86
1.5	102.57	104.05	1.4
2.1	113.9	107.20	6.24
2.7	124 .84	112.7	10.78

Table.2: Total heat removal rate and radiative heat rate for different cases

Case of DHW	500°C	400°C	300°C	200°C	100°C	50°C
$\dot{Q}_{removal\ ,num}$ (kW)	5.90	4.07	2.3	1.13	0.30	0.095
$\dot{Q}_{removal\ ,exp}$ (kW)	6.05	3.7	2.2	1.08	0.27	0.1
Error %	2.47	10	4.5	4.6	11	5
$\dot{Q}_{rad\ ,num}$ (kW)	1.56	0.84	0.42	0.17	0.044	0.014
$\dot{Q}_{rad\ ,exp}$ (kW)	1.70	0.75	0.4	0.18	0.04	0.015
Error %	8	12	5	5	10	6

Figures 2.a and 2.b illustrate the numerical results for the total heat removal rate and radiative heat rate over time, respectively, for each wall temperature case. It can be observed that steady-state conditions are reached within 30 seconds, and the numerical results closely match the experimental data during this time. Furthermore, Table 2 provides more evidence of the conformity between the numerical and experimental results. Figure 3 depicts the numerical results of the Nusselt number versus Rayleigh number, showing good agreement with the experimental results of K. M. Kim et al. [14].

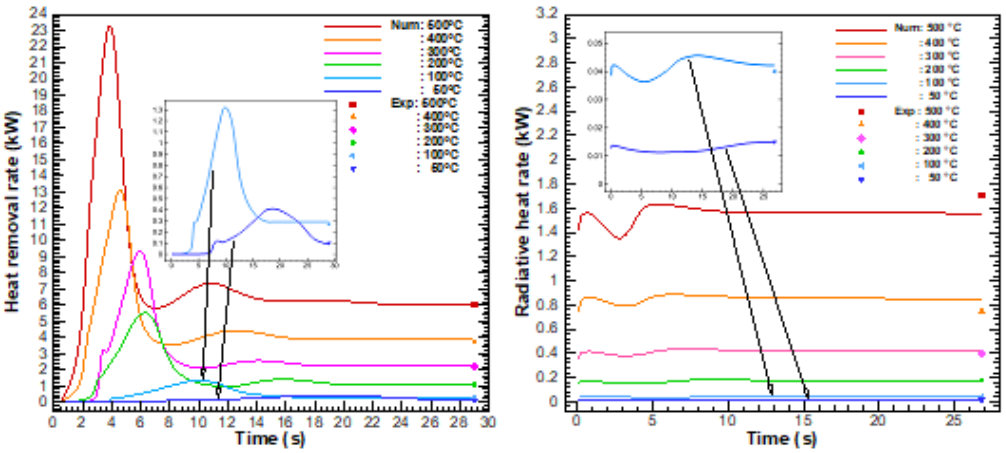

Figure 2.a: Total heat removal rate, **Figure 2.b: Radiative heat rate**

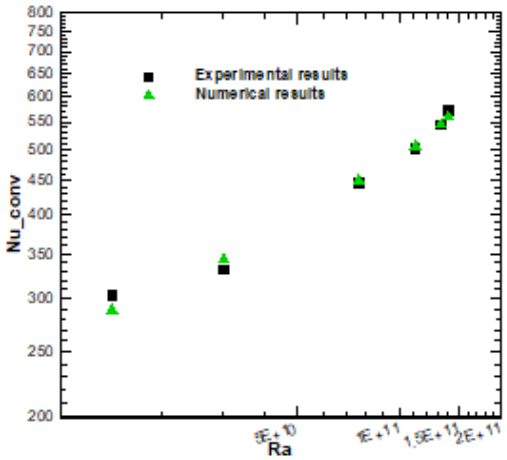

Figure 3: Experimental and numerical Nusselt versus Rayleigh number

Figure 4 illustrates the calculated profiles of the air temperature at different heights of the channel for each case of the DHW. Across all cases, a sharp decline in air temperature is observed as the distance from the DHW increases. However, the air temperature experiences resurgence near the IHW, attributed to thermal radiation. With an increase in height, the influence of the wall's higher temperature extends, elevating the air temperature in the channel's core above that at lower heights. The air temperature in the central region is clearly higher than the inlet air temperature (15-25°C). Notably, the lowest air temperature is recorded near the IHW at a height of 0.9 m, progressively shifting towards the channel's center with rising elevation. It is observed that as the temperature of the DHW increases, the temperature of the IHW also rises, owing to the effects of thermal radiation.

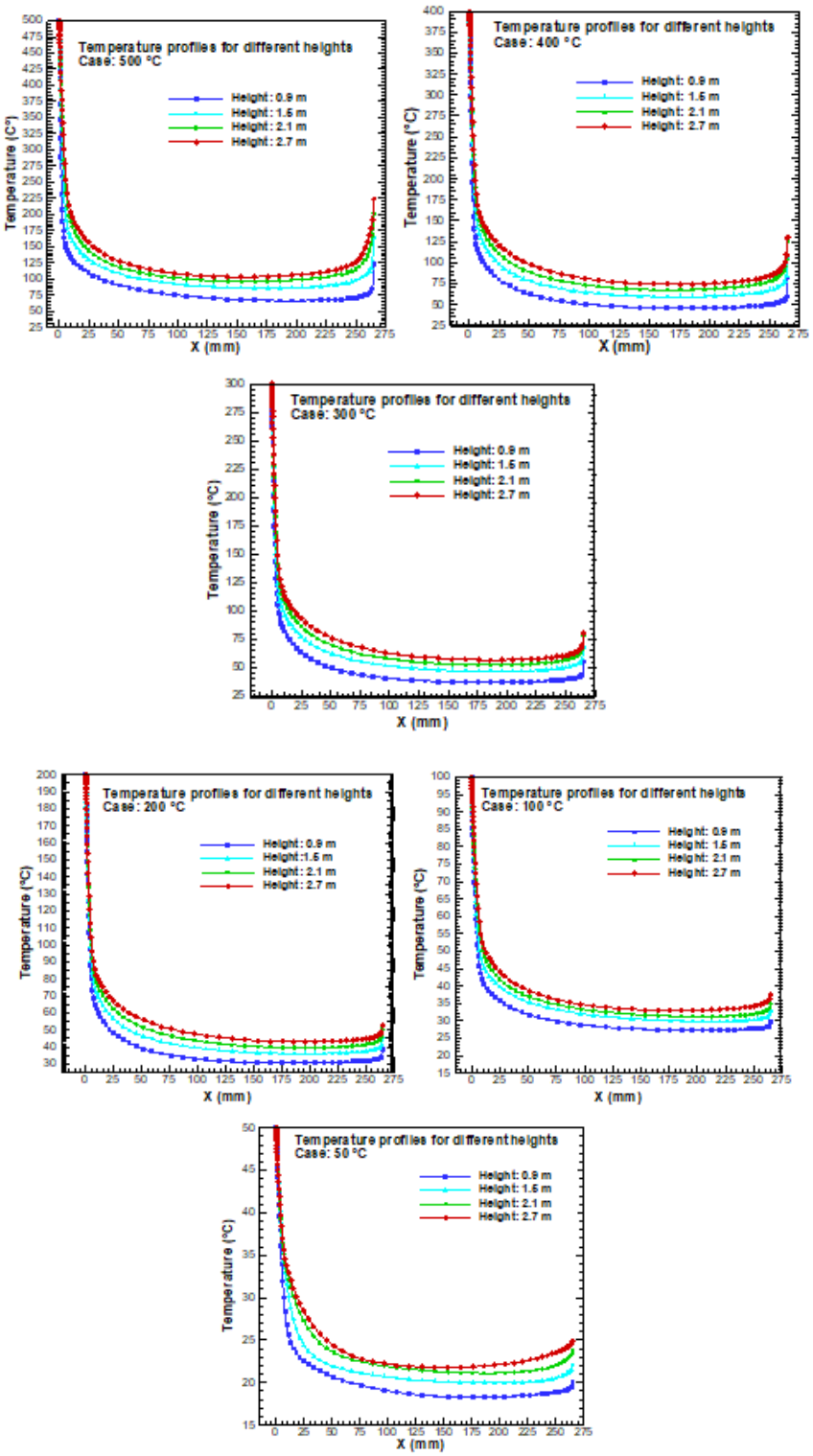

Figure 4: Numerical temperature profiles at different heights and for different cases

Figure 5 depicts the calculated profiles of the air velocity at different heights of the channel for each case of the DHW. Analogous trends are noted for air velocity; the peak velocity occurs near the surface of the DHW, a characteristic of natural convection. Then, velocity decreases gradually as the distance from the DHW increases. Distinct inflection points are discernible near the IHW, particularly pronounced in the cases with DHW temperatures of 400 °C and 500 °C and at an

elevation of 2.7 m, where a slight uptick in temperature is recorded, culminating in a secondary peak, which can be attributed to the effects of thermal radiation. When considering a lower temperature for the DHW, particularly in the case of 50°C, the velocity profile exhibits a notable trend. The velocity diminishes to its minimal value, approaching zero. At a height of 0.9 m, the velocity profile takes an intriguing turn, becoming negative. This indicates a reversal in the direction of airflow, which is a significant observation in the study of convective heat transfer phenomena.

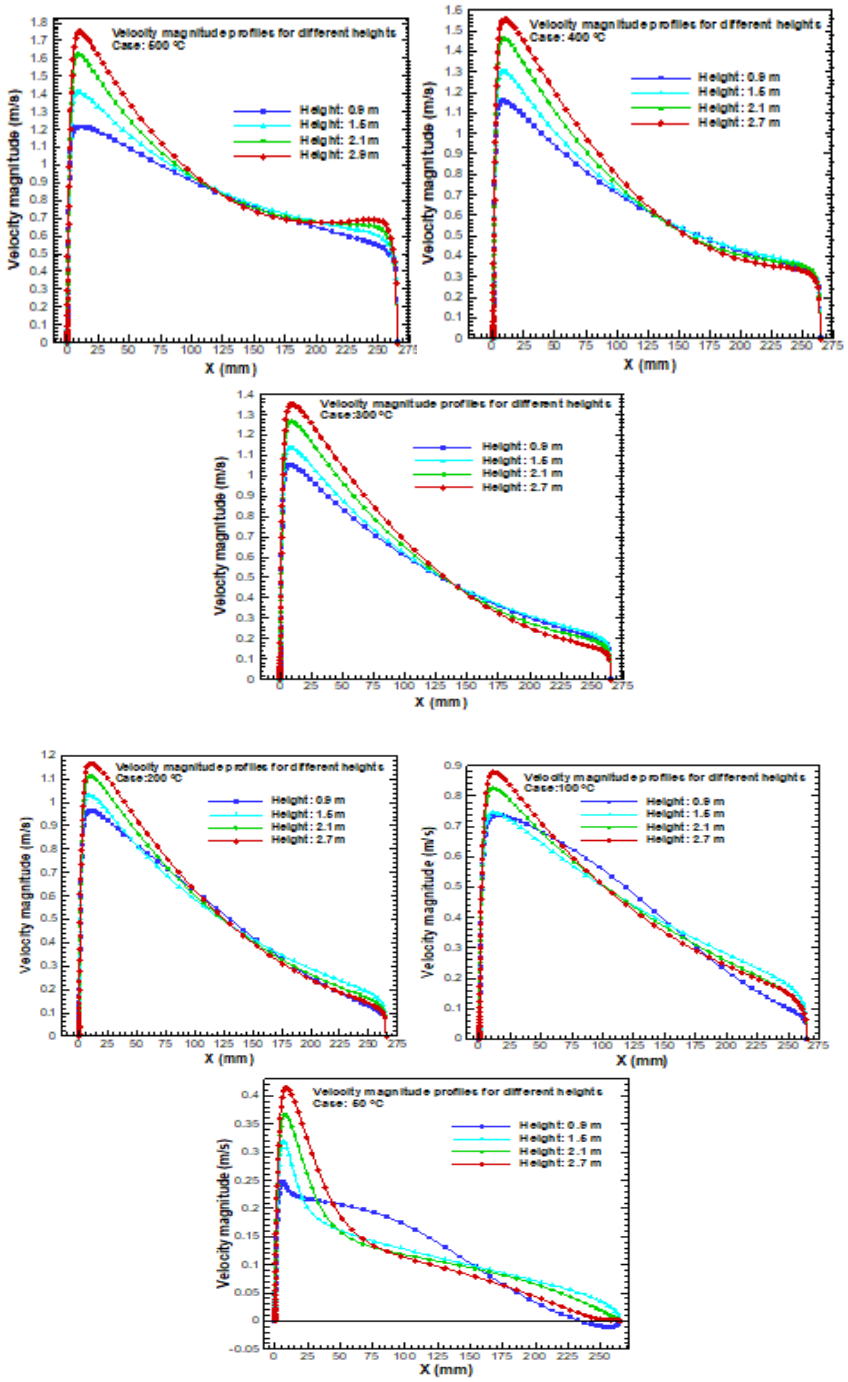

Figure 5: Numerical velocity profiles at different heights and for different cases

Figure 6 displays the temperature contours within the U-shaped channel, showcasing different DHW temperatures. It's clear that the isothermal temperature profiles deviate from symmetrical

parabolic shapes due to the temperature difference between the two heated walls, as discussed earlier in the section on temperature profiles (see figure 4). This asymmetry is particularly pronounced at lower elevations, where the temperature gap between the two walls is more significant, particularly for cases with higher DHW temperatures. In fact, as depicted in Figure 4, the lowest air temperatures at low elevations are found adjacent to the side wall that receives thermal radiation. With an ascent in height, this zone of minimal temperature gradually transitions towards the central axis of the channel. Naturally, the outlet temperature of the air is higher for higher DHW temperatures due to enhanced natural convection. Table 3 summarizes the outlet temperatures (based on the area-weighted average) corresponding to the inlet temperatures for each case.

Table.3: Numerical average inlet and outlet temperature for each case

Case of DHW	500°C	400°C	300°C	200°C	100°C	50°C
Average outlet temperature (°C)	125	87	70	62	42	25
Average inlet temperature (°C)	25	25	23	23	25	15

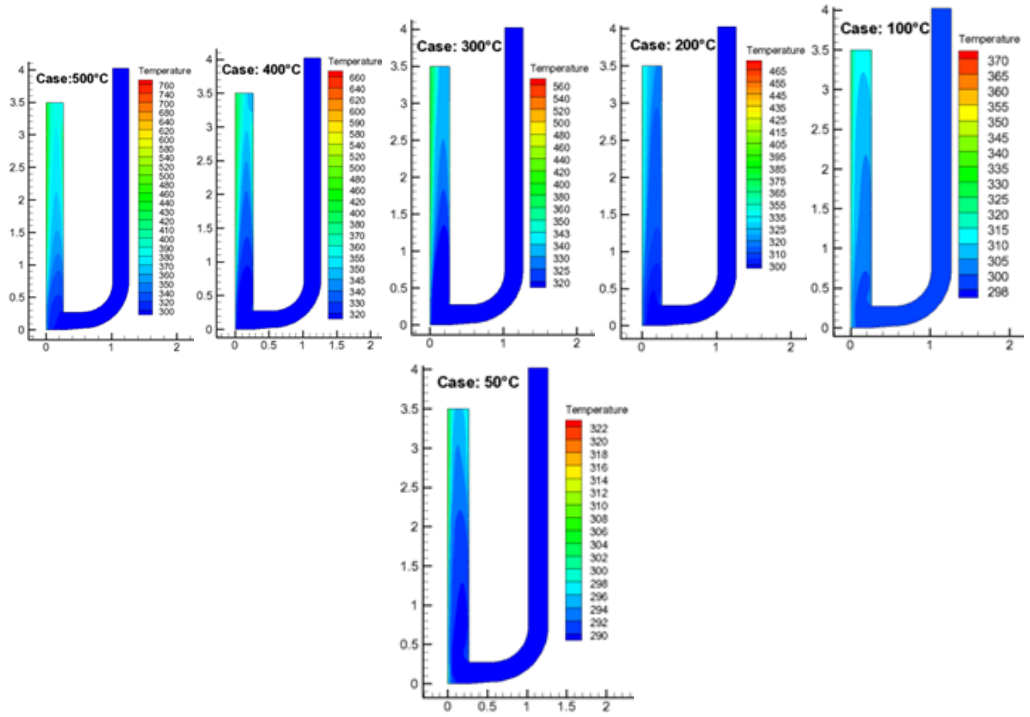

Figure 6: Contours of temperature for different cases.

Figure 7 depicts the streamlines and velocity magnitude contours for each case of the DHW temperatures. The flow velocities appear to be nearly uniform throughout the channel in all cases. It's evident that the velocity magnitude is significantly higher at the DHW region and gradually decreases as it approaches the IHW region.

However, two regions of recirculation with low velocity magnitude are noticeable. One recirculation flow forms near the IHW, and another one develops near the corner edge of the DHW. These recirculation regions are a result of the strong flow induced by the buoyancy force at the DHW. The surrounding air is drawn from the horizontally installed inlet, concentrating and reflecting the airflow at the DHW due to inertia. This phenomenon was previously suggested by K. M. Kim et

al. [14] in their experimental study. These two regions are more pronounced in the case of lower DHW temperatures, specifically for the 50°C case. In this case, the recirculation flow develops near the IHW, reaching a height of 1.1 m within the channel. As the temperature of the DHW increases, the size of these two regions becomes smaller until they disappear for the DHW of 500°C case. Additionally, it should be noted that both average velocity magnitude at the inlet and at the outlet increase significantly as the DHW temperature rises, as mentioned in Table 4.

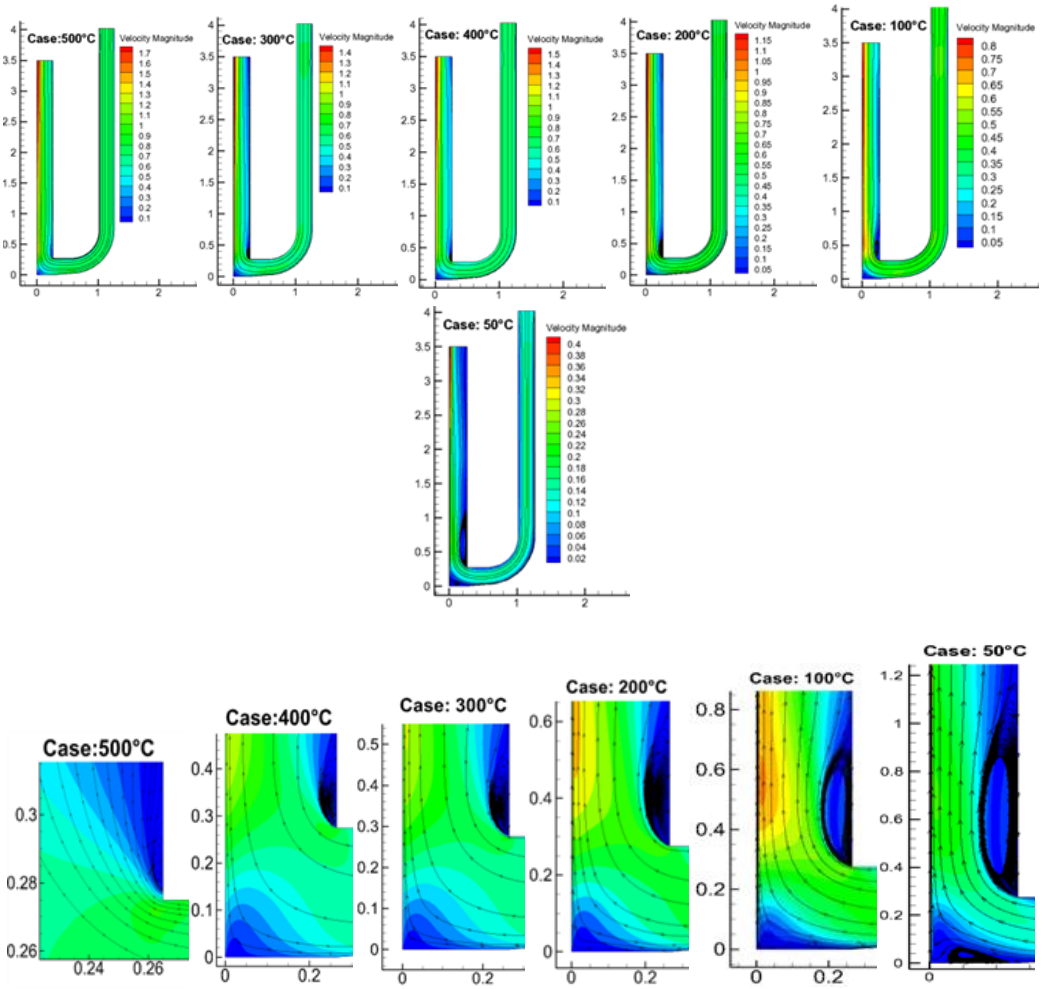

Figure 7: Contours of velocity magnitude for different cases

Case of DHW	500°C	400°C	300°C	200°C	100°C	50°C
Average velocity inlet (m/s)	1.169	1.032	0.698	0.579	0.529	0.26
Average velocity outlet (m/s)	1.279	1.230	0.806	0.608	0.532	0.25

Figure 8 presents the relationship between the convective Nusselt-number and the Rayleigh-number, as determined directly from the numerical results. The numerical results align well with the following equation:

$$Nu_{conv} = 0.1\ Ra^{1/3}$$

This equation aligns closely with the findings of previous studies by Cheng and Müller [9] and K. M. Kim et al. [14]. These studies found a similar correlation to that of turbulent natural convection in a single infinite vertical plate, as reported by S.W. Churchill and H.H. Chu [18]. This correlation becomes apparent when the aspect ratio (S/H) surpasses 0.032, at which point the heat transfer behavior between vertical parallel plates begins to resemble that of a single vertical plate.

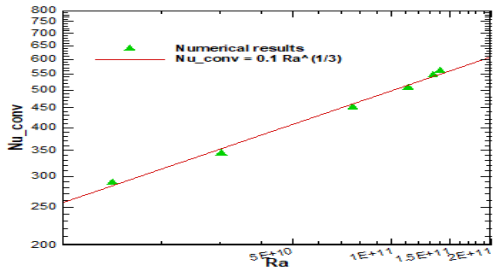

Figure 8: Numerical Nusselt versus Rayleigh number for different

4. Conclusion

This paper presents a numerical simulation of turbulent air natural convection in a U-shaped channel with asymmetric heating conditions. The numerical results were validated against existing experimental measurements and showed good agreement. The study investigated the impact of different DHW temperatures on various parameters, including: Heat removal rate, Nusselt number, air temperature, and air velocity through the channel. The air temperature profiles exhibited a sharp decline with increasing distance from the DHW, followed by resurgence near the IHW due to thermal radiation. The air temperature in the central region was significantly higher than the inlet air temperature. The air velocity profiles displayed a peak near the DHW surface, followed by a gradual decrease. Distinct inflection points were observed near the IHW, particularly for higher DHW temperatures. The isothermal temperature profiles deviated from symmetrical parabolic shapes due to the temperature difference between the heated walls. The flow velocities were nearly uniform throughout the channel, with higher magnitudes near the DHW and lower magnitudes near the IHW. Two recirculation regions were observed, one near the IHW and another near the corner edge of the DHW. These regions were more pronounced at lower DHW temperatures. Finally, this study provides valuable insights into the turbulent air natural convection in a U-shaped channel with asymmetric heating conditions. The findings can be applied to optimize the design of natural convection systems in various applications, such as chimneys, heat sinks, and radiators.

Latin symbols	*Greek symbols*
A, Area , m^2	ρ fluid density, kg/m
C_p specific heat coefficient, $Jkg^{-1}\ K^{-1}$	μ dynamic viscosity, Pa.s
DHW Directly Heated Wall	μ_t turbulent viscosity, Pa.s
DO discrete ordinates radiation model	σ_k turbulent Prandtl number for k
h average convective heat transfer coefficient, $W/m^2.K$	β Thermal expansion coefficient, 1/K

H Height of the channel, m

IHW Indirectly Heated Wall

k turbulent kinetic energy, m^2/s^2

$\dot{m}$ mass flow rate, kg/s

Nu Nusselt number

P pressure, Pa

P_o operating pressure, Pa

Pr Prandtl number ($=\mu C_p/\lambda$)

Pr_t turbulent Prandtl number

Ra rayleigh number

r_{air} air constant, $JK^{-1}kg^{-1}$

S gap size between the heated walls, m or strain rate, s^{-1}

T temperature, K

u x component velocity, m/s

v y component velocity, m/s

ν kinematic viscosity, m^2/s

σ_ε turbulent Prandtl number for ε

ε turbulent energy dissipation, m^2/s^3

λ conductivity coefficient, $Wm^{-1}\ K^{-1}$

ϵ emissivity

σ Stefan-Boltzmann constant, $W/m^2.K^4$

Subscripts

0 initial condition

avgaverage

in inlet

out outlet

w wall

References

[1] W.Elenbaas, Heat dissipation of parallel plates by free convection, Physica 9 (1) (1942) 1–28.

[2] J.R. Bodoia, J.F. Osterle, the Development of Free Convection between Heated Vertical Plates, Journal of Heat Transfer 84 (1) (1962) 40–43.

[3] S.Ostrach, Laminar natural convection flow and heat transfer of fluids with and without heat sources in channels with constant wall temperatures, NACA TN 2863 (1952).

[4] W.Aung, Fully developed laminar free convection between vertical plates heated asymmetrically.Orf.J.Heat Mass Transfer 15, 1577F1580 (1972).

[5] O. Miyatake, T. Fujii, M. Fujii and H. Tanaka, Natural convective heat transfer between vertical parallel plates-one plate with a uniform heat flux and the other thermally insulated, Heat Transfer-Jap. Res 2, 25-33 (1973).

[6] D.J.Nelson, B.D.Wood, Fully developed combined heat and mass transfer natural convection between parallel plates with asymmetric boundary conditions, International Journal of Heat and Mass Transfer, Volume 32, Issue 9,1989, 1789-1792.

[7] T. Yilmaz, A. Gilchrist, Temperature and velocity field characteristics of turbulent natural convection in a vertical parallel-plate channel with asymmetric heating, Heat Mass Transfer (2007) 43:707–719.

[8] A. Bar-Cohen, W.M. Rohsenow, Thermally Optimum Spacing of Vertical, Natural Convection Cooled, Parallel Plates, Journal of Heat Transfer 106 (1) (1984) 116–123.

[9] X. Cheng, U. Müller, Turbulent natural convection coupled with thermal radiation in large vertical channels with asymmetric heating, Int. J. Heat Mass Transf. 41 (12) (1998) 1681–1692.

[10] J. Cadafalch et al, Natural convection in a large, inclined channel with asymmetric heating and surface radiation, J. Heat Transfer. Oct 2003, 125(5): 812-820.

[11] G. Desrayaud and A. Fichera, Laminar natural convection in a vertical isothermal channel with symmetric surface-mounted rectangular ribs, International journal of heat and fluid flow 23 (2002) 519–529.

[12] R. Khanal and C. Lei, Flow reversal effects on buoyancy induced air flow in a solar chimney, Solar Energy 86 (2012) 2783–2794.

[13] G. Gan, General expressions for the calculation of air flow and heat transfer rates in tall ventilation cavities, Building and Environment, 46 (2011) 2069-2080.

[14] K. M. Kim, Experimental study of turbulent air natural convection in open-ended vertical parallel plates under asymmetric heating conditions, International Journal of Heat and Mass Transfer 159 (2020) 120135.

[15] A.Shitzer, Wind-chill-equivalent temperatures: regarding the impact due to the variability of the environmental convective heat transfer coefficient, Int J Biometeorol (2006) 50: 224–232.

[16] V.S.Touloukian, D.P. DeWitt, Thermal radiativeproperties-Metallic Elements and Allays, Springer Science+ Business Media, LLC 1970.

[17] ANSYS Inc. Fluent User Guide and Fluent Theory Guide, Version 13.0, 2010

[18] S.W. Churchill, H.H. Chu, Correlating equations for laminar and turbulent free convection from a vertical plate, Int. J. Heat Mass Transf. 18 (11) (1975) 1323–1329.

[19] Mehran Ahmadi et al., Natural Convection from Vertical Parallel Plates: An Integral Method Solution, Journal of thermophysics and heat transfer vol. 29, no. 1, january–march 2015

[20] Alessandro Quintino et al., Dimensionless Correlations for Natural Convection Heat Transfer from a Pair of Vertical Staggered Plates Suspended in Free Air, Appl. Sci. 2021, 11(14), 6511.

[21] Qi Liu et al., Numerical Investigation of Natural Convection in an Open-Ended Square Channel with Two Suspending Heat Sources" Processes 2022, 10(9), 1774 .